

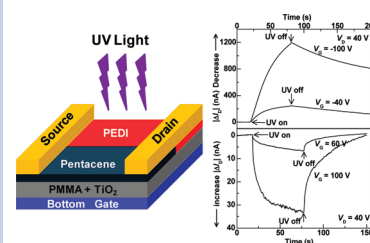
# Mirror-Image Photoswitching in a Single Organic Thin-Film Transistor

Qian Shen, Yang Cao, Song Liu, Lin Gan, Jianming Li, Zhenxing Wang, Jingshu Hui, Xuefeng Guo,\* Dongsheng Xu, and Zhongfan Liu\*

Beijing National Laboratory for Molecular Sciences, State Key Laboratory for Structural Chemistry of Unstable and Stable Species, College of Chemistry and Molecular Engineering, Peking University, Beijing 100871, People's Republic of China

**ABSTRACT** In this study, we detailed our design for making a photoactive semiconductor/dielectric interface in order to study charge dynamics at the interface in combination with photoexcitation, using organic thin-film transistors (OTFTs) as local probes. The photoactive semiconductor/dielectric interface is formed from a hybrid gate dielectric (polymethyl methacrylate (PMMA) and titanium oxide (TiO<sub>2</sub>)). Because the photogenerated electrons from TiO<sub>2</sub> nanoparticles under UV illumination can serve as the trapping centers for quenching hole carriers, p-type semiconductors showed the decrease of the hole mobility. Interestingly, n-type semiconductors displayed symmetric, opposing photoswitching effects at the same condition, showing that the photogenerated holes can function as a local positive gate voltage for improving the electron mobility. On the basis of this understanding, a remarkable example of mirror-image photoswitching effects in a single ambipolar OTFT was realized. These results may offer grounds for the creation of the future practical/multifunctional organic optoelectronic devices.

**SECTION** Electron Transport, Optical and Electronic Devices, Hard Matter



**Scheme 1.** (a) Schematic of Typical "Top-Contact" OTFTs Showing That Charge Transport Is through, at Most, the First Few Layers of Molecules at the Semiconductor/Dielectric Interface and (b) Schematic of the Device Structure Used in This Study Showing How TiO<sub>2</sub> Nanoparticles Affect the Device Characteristics at the Semiconductor/Dielectric Interface under UV Irradiation

Organic thin-film transistors (OTFTs), as one of the fundamental building blocks in electronic circuits, were the subject of extensive research in the past decade because of their potential advantages, such as solution-processability, light weight, the possibility of large-area processing, low cost, and flexibility.<sup>1–4</sup> Through the development of novel high-performance organic semiconductors and device optimization, transistor performance has been significantly improved.<sup>1–10</sup> The field-effect mobility of OTFTs is already comparable to that of devices formed from amorphous silicon, and OTFTs are on the verge of commercialization. However, there are still many fundamental challenges due to the poor understanding of the conduction mechanisms in OTFTs.<sup>5–16</sup> For example, for the practical applications of OTFTs, the key remaining problems are the device reliability and operational stability. Overcoming these challenges relies on rational control of charge trapping/detrapping at the semiconductor/dielectric interface<sup>6,9,10,17,18</sup> or contact regions.<sup>19,20</sup> In addition, deeper understanding of the trap dynamics at the semiconductor/dielectric interface should also help to improve device performance, reduce the power dissipation and fabrication cost, explore new functionality, and develop simple fabrication techniques.<sup>6,9,10,17–25</sup>

In typical "top-contact" OTFTs, previous studies have shown that charge transport occurs through at most the first few layers of molecules at the semiconductor/dielectric interface (Scheme 1a).<sup>26,27</sup> Therefore, the property of this interface plays an important role in device characteristics. Any

small changes from the interface could cause drastic changes to the electrical properties of devices. Modifications of the semiconductor/dielectric interface are now under intense investigation and may provide an efficient approach to improving the device performance and/or installing new functionalities. In this study, we demonstrated our recent design

**Received Date:** March 5, 2010

**Accepted Date:** March 25, 2010

**Published on Web Date:** March 29, 2010

for making a photoactive semiconductor/dielectric interface in order to understand the charge dynamics at the interface in combination with photoexcitation using OTFTs as local probes. The photoactive semiconductor/dielectric interface is formed from a hybrid gate dielectric, which is composed of a buffer polymer carrier, polymethyl methacrylate (PMMA), and a photoresponsive nanoparticle, titanium oxide ( $\text{TiO}_2$ ).  $\text{TiO}_2$  has been extensively investigated owing to its widespread applications in photocatalysis and many other studies.<sup>28,29</sup> Particularly relevant to our design are the studies of Lee, Yan, Cho, and their co-workers, which show that  $\text{TiO}_2$  nanoparticles when simply mixed with the gate dielectric or organic semiconductors can improve the device performance and/or build photosensitive organic transistors.<sup>30–32</sup> Interestingly, when UV light was switched on/off, we were able to reversibly perform the detailed dynamical study of charge trapping/detrapping processes at the semiconductor/dielectric interface and consequently fine-tune the device characteristics of both p-type and n-type OTFTs in the opposite directions. Importantly, rational control of charge trapping/detrapping at the interface allows us to realize a remarkable example of the mirror-image photoswitching effect in a single ambipolar OTFT.

OTFTs with typical top-contact, bottom-gate geometries were fabricated by a standard procedure through thermal evaporation (see Supporting Information). To maximize the effect of  $\text{TiO}_2$  nanoparticles on the electronic properties of devices, we used highly doped silicon wafers without silicon oxide layers as the substrates (Scheme 1b). The 1200 nm thick hybrid gate dielectrics were formed from the PMMA solution of  $\text{TiO}_2$  nanoparticles at the saturation concentration of  $\sim 1 \times 10^{-5}$  g/mL through spin-coating and dried under vacuum condition at room temperature overnight. We chose the hybrid PMMA dielectrics with 1200 nm thickness because we found that the photoresponsive behaviors of the devices were independent of the dielectric thickness, as discussed below, and this thickness of hybrid PMMA dielectrics affords gate leakage current densities ( $J_{\text{leak}}$ ) below levels that affect OTFT properties ( $J_{\text{leak}} < 10^{-8}$  A/cm<sup>2</sup> at a gate field of  $\sim 1$  MV/cm). Figure S1a (Supporting Information) shows an atomic force microscopic (AFM) image of surface morphologies of the hybrid gate dielectrics. As can be seen, discrete  $\text{TiO}_2$  nanoparticles were observed on the surface. The average size of these nanoparticles is  $\sim 1.2$  nm in height and  $\sim 70$  nm in diameter. This explains that  $\text{TiO}_2$  nanoparticles show slight aggregation during the dispersion into the PMMA solution in comparison with the diameter of individual  $\text{TiO}_2$  nanoparticles (3–5 nm) (Figure S2, Supporting Information), and only a small part of the aggregates sticks out from the surface. It is these convex  $\text{TiO}_2$  nanoparticles that make the main contribution to the photoresponsive behaviors of OTFTs discussed below. UV/visible absorption studies demonstrated that solution-cast thin films of  $\text{TiO}_2$  nanoparticles from hexane on quartz substrates show reversible optical absorption changes in the range of 230–300 nm under UV irradiation ( $\lambda = 254$  nm) and in the dark (Figure S1b, Supporting Information). These reversible spectral changes of  $\text{TiO}_2$  nanoparticles are a harbinger for the useful optoelectronic properties described below. After 40 nm organic thin-film deposition via thermal

evaporation (pentacene or *N,N*-dihexylperylene diimide (PEDI)), this hybrid polymer dielectric allowed us to obtain very large pentacene crystal grains ( $\sim 3\text{--}4$   $\mu\text{m}$ ) with terraces (step heights about 15 Å) and PEDI thin films with uniform and densely packed structures, as demonstrated by AFM (Figure S3, Supporting Information). In addition, X-ray diffraction measurements demonstrated the formation of highly crystal quality organic thin films on top of the dielectric (Figure S4, Supporting Information). These results are important to achieve the optimal OTFT performance.

After surface structure characterization, top-contact source and drain electrodes (40 nm Au) were deposited onto organic thin films through a metal shadow mask. The 1200 nm dielectric films were electrically characterized by using the sandwich electrode structures with gold pads (0.9 mm<sup>2</sup>) on their surface. The measured capacitance value ( $C_i$ ) was  $\sim 2.4$  nF/cm<sup>2</sup> and remained constant under UV irradiation and in the dark. We first explored the details of charge trapping/detrapping dynamics at the semiconductor/dielectric interface in p-type OTFTs. Figure 1 shows the comparison of the transistor characteristics of a representative pentacene field-effect transistor before and after UV illumination. Both output and transfer characteristics exhibit classical linear/saturation behaviors in both cases. Noticeably, after UV irradiation for  $\sim 24$  s, dramatic decreases in drain current ( $I_D$ ) occurred, regardless of the gate bias (Figure 1). The incident UV light generated free electron–hole pairs in the  $\text{TiO}_2$  nanoparticles.<sup>28,29</sup> As hypothesized by Dittrich et al.,<sup>33</sup> the photogenerated holes are easily trapped on the surface of  $\text{TiO}_2$  nanoparticles. On the contrary, the photogenerated electrons have a significant mobility in  $\text{TiO}_2$  nanoparticles and could penetrate through the dielectric layer to the semiconductor/dielectric interface, as demonstrated by an increase of the gate leakage current during irradiation (not shown). Consequently, the current decrease in the pentacene transistors is explained by the photogenerated electrons at the interface that behave like a Coulomb trap and quench the p-type carriers in the devices. These results are in agreement with those from earlier work on photoinduced charge transfer at the semiconductor/dielectric interface by Calhoun.<sup>34</sup> A relatively less negative shift of the onset voltage ( $V_O$  from  $-2.5$  to  $-12.0$  V in Figure 1b and d) was observed in the current case in comparison with that from their work ( $> 40$  V) probably due to the decreased number of photogenerated Coulomb traps from  $\text{TiO}_2$  nanoparticle surfaces, as discussed below. Remarkably, when kept in the dark after UV irradiation, the device presented a very slow current relaxation, and its drain current was essentially restored to its original value. This can be explained by the progressive detrapping of holes on the surface of  $\text{TiO}_2$  nanoparticles by electrons that originate from the conductive channel where the p-type transistors have a very low density of electrons. We found that the back-and-forth charge trapping/detrapping effect is rather gradual in time. Figure 2a and b shows the time evolution of the current–voltage curves during UV illumination and in the dark, respectively. The drain current sharply decreased at the beginning of UV irradiation and was saturated after  $\sim 24$  s of exposure when  $\text{TiO}_2$  nanoparticles reached the maximum of photogenerated charge separation (Figure 2a). On the

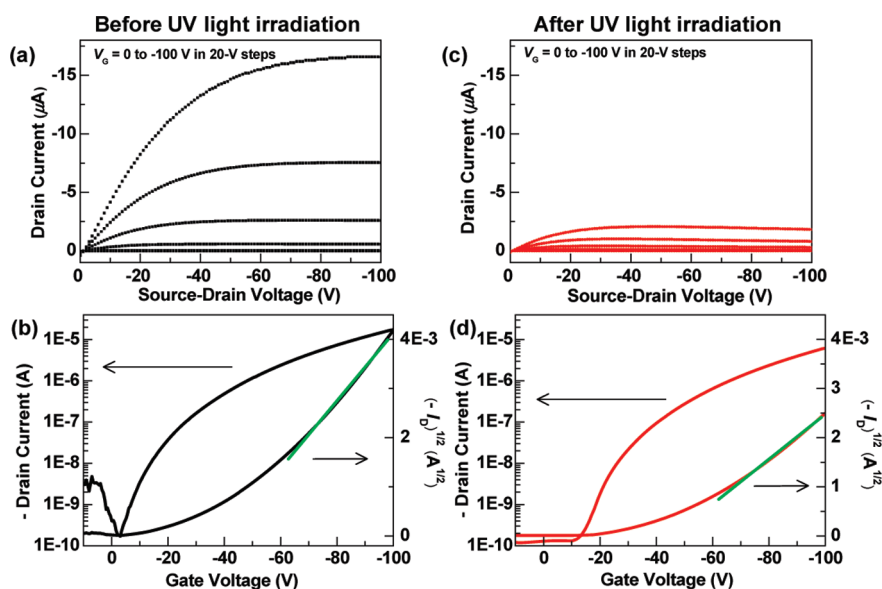


**Figure 1.** Device characteristics of a pentacene device before and after UV irradiation. (a) Transistor output before UV irradiation,  $V_G = 0$  to  $-100$  V in 20 V steps. (b) Transfer characteristics before UV irradiation,  $V_D = -100$  V. (c) Transistor output after UV irradiation,  $V_G = 0$  to  $-100$  V in 20 V steps. (d) Transfer characteristics after UV irradiation,  $V_D = -100$  V.

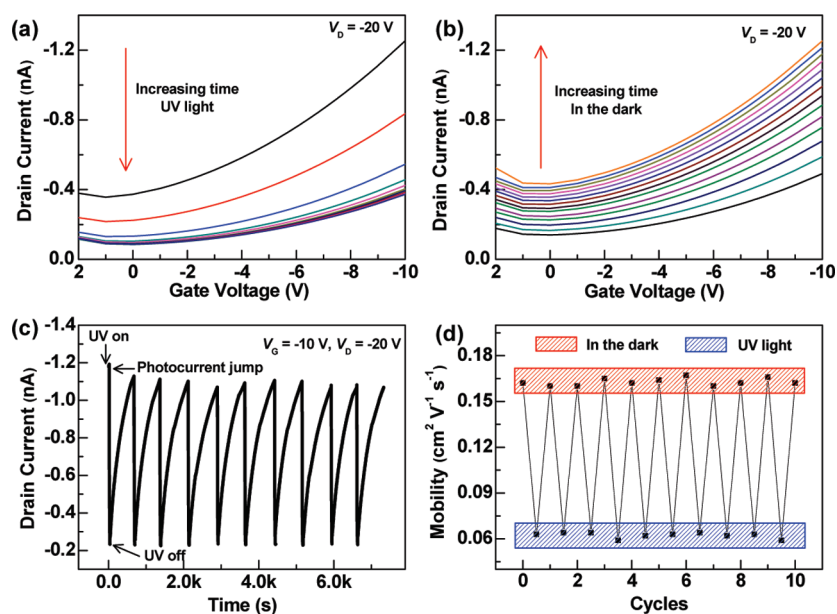


**Figure 2.** (a, b) The gradual charge trapping/detrapping processes of the device used in Figure 1 when the curves were taken every 2.5 s for UV illumination and every 1 min in the dark.  $V_D = -20$  V. (c) Time trace of  $I_D$  for the same device, showing the reversible charge trapping/detrapping processes when UV light was switched on/off.  $V_D = -20$  V, and  $V_G = -10$  V. (d) The corresponding representative switching cycles of the mobility of the same device.

contrary, after the low-conductance state was established and the device was kept in the dark, the drain current of the same device sharply increased initially and then slowly attenuated, completing the increase after  $\sim 12$  min (Figure 2b).

To quantify the dynamics for the charge trapping/detrapping process, we monitored the drain current as a function of time ( $V_D = -20$  V,  $V_G = -10$  V) as UV irradiation was toggled between on and off. Figure 2c shows 10 dynamic cycles of the time-dependent behaviors of the same device. The expanded

part for one full cycle of the behaviors can be found in the Supporting Information (Figure S5). These behaviors are consistent with the results from Figure 2a and b. A sudden current jump ( $\sim 7\%$  in the total current change) was observed at the moment of turning on UV light generally due to the photoexcited state of organic semiconductors, as proven by control experiments in Figure S6 (Supporting Information). As shown in Figure 2c, all of the functioning OTFTs are quite stable and can endure the long-term operation in ambient

atmosphere without obvious degradation. The kinetics of each process can be fit with a single exponential. On the basis of the data from Figure 2c, the overall rate constants in different parts were calculated,  $K_{(\text{UV})} = \sim 0.16 \pm 0.02 \text{ s}^{-1}$  and  $K_{(\text{dark})} = \sim 3.9 \pm 0.2 \times 10^{-3} \text{ s}^{-1}$ . To prove the importance of  $\text{TiO}_2$  nanoparticles in the charge trapping/detrapping process, we performed control experiments in which we measured the photoresponse of a pentacene device having the same PMMA dielectric but lacking  $\text{TiO}_2$  nanoparticles. Figure S6 (Supporting Information) shows the drain current characteristics of such a device as a function of time under the same measurement conditions. With UV light either on or off, we consistently observed the slow decrease in drain current, probably resulting from problems associated with the device stability. From the trace in Figure S6 (Supporting Information), the overall rate constants for each part were obtained,  $K_{(\text{UV})} \approx K_{(\text{dark})} = \sim 3.0 \pm 0.1 \times 10^{-3} \text{ s}^{-1}$ . In comparison with those in functioning devices, two significant differences should be pointed out. One is that the rate constant of the device in Figure 2c under UV irradiation is 2 orders of magnitude larger than that obtained from the control device in Figure S6 (Supporting Information). The other significant difference is that the photoresponse of the functioning devices at UV light turn-off is opposite to that in the control devices. Consequently, it is quite clear that the photogenerated charge separation of  $\text{TiO}_2$  nanoparticles is responsible for the charge trapping/detrapping process in our devices.

It should be noted that, although the FET characteristics of the devices gradually became worse with the thickness increase of hybrid gate dielectrics (from 150 to 300, 600, and 200 nm), no obvious relation was found between the dielectric thickness and the photoswitching characteristics of the devices. This strengthens the above-mentioned hypothesis that the charge trapping/detrapping processes at the semiconductor/dielectric interface lead to the reversible photoswitching of device characteristics in the current case. To further validate this hypothesis, we designed and tested three sets of control experiments. The current–voltage curves for these control experiments can be found in the Supporting Information (Figure S7–9). A first experiment tested the electrical characteristics of devices with PMMA (bottom, 1200 nm)/ $\text{TiO}_2$  (top, 40 nm through e-beam thermal evaporation) bilayer dielectrics. The current–voltage curves showed similar changes when UV light was toggled between on and off because an effective interface was formed between  $\text{TiO}_2$  and pentacene thin films. The much lower back-conversion of  $I_D$  in the dark was observed because of the higher trap density on the surface of  $\text{TiO}_2$  thin films in comparison with devices with hybrid gate dielectrics used above. A second experiment, which tested the devices with only the 1200 nm PMMA dielectric but coated by a 40 nm  $\text{TiO}_2$  thin film on top of pentacene also showed the similar changes in device characteristics. The third experiment, in which we used devices with  $\text{TiO}_2$  (bottom, 40 nm)/PMMA (top, 1200 nm) bilayer dielectrics, did show essentially no changes in device characteristics under UV irradiation and in the dark. This is because the devices lack the photoactive semiconductor/dielectric interface and the photogenerated electrons are

unable to reach the interface through thick PMMA films. This is very important and consistent with that in capacitance measurements mentioned above, which have proved that the capacitance of hybrid gate dielectrics remains constant under UV irradiation and in the dark.

It is remarkable to note that the rational utilization of generally detrimental charge trapping/detrapping at the semiconductor/dielectric interface allows us to fine-tune the electrical characteristics of the devices. On the basis of the data from the device used in Figure 1, we can calculate the corresponding field-effect mobilities. As shown in Figure 2d, the device nicely switched its mobility back and forth between two distinct states. Interestingly, we can extract the concentration ( $N$ ) of the photogenerated Coulomb traps in  $\text{TiO}_2$  nanoparticles at the interface by using a simple model for the calculation,  $N = C_i \Delta V_O / e$ , where  $\Delta V_O$  is the shift of the onset voltage ( $V_O$ ) and  $e$  is the elementary charge.<sup>34</sup> Using a value of  $\Delta V_O = 9.5 \text{ V}$  obtained above, we estimate that approximately  $1.4 \times 10^9$  Coulomb traps  $\text{cm}^{-2}$  are filled at the interface after UV illumination (much less than  $3 \times 10^{11}$  Coulomb traps  $\text{cm}^{-2}$  obtained in ref 10). This value is also less than those obtained under the same conditions from control experiments with bulk  $\text{TiO}_2$  thin films ( $\sim 1.9 \times 10^{10}$  Coulomb traps  $\text{cm}^{-2}$  for the first control experiment and  $\sim 2.2 \times 10^{10}$  Coulomb traps  $\text{cm}^{-2}$  for the second control experiment). This moderate value is important for achieving the optimal device performance and photoswitching properties.

We then turned our attention to the dynamical study of charge trapping/detrapping processes in an n-type PEDI OTFTs. Figure S10 (Supporting Information) shows the comparison of the transistor characteristics of a representative PEDI field-effect transistor before and after UV illumination. Surprisingly, after UV irradiation for  $\sim 30 \text{ s}$ , significant increases in drain current ( $I_D$ ) were observed at any gate bias (Figure S10, Supporting Information). This is completely opposite to the results observed in p-type pentacene OTFTs. These results are reasonable because photogenerated free electrons of  $\text{TiO}_2$  nanoparticles at the semiconductor/dielectric interface can move toward the gate electrode under a positive gate bias and leave the holes trapped inside of  $\text{TiO}_2$  nanoparticles at the interface. These trapped holes act as a local positive gate voltage, thus improving the electron mobility. This also results in the shift of the onset voltage toward the on-state ( $V_O$  from 31 to 27 V) (Figure S10, Supporting Information). Figure 3a shows the dynamics of the charge trapping/detrapping process of the same device as that used in Figure S10 (Supporting Information). We measured the drain current as a function of time ( $V_D = 50 \text{ V}$ ,  $V_G = 50 \text{ V}$ ) as the UV light was switched on/off. The kinetics of each process can be also fit with a single exponential. On the basis of the data from Figure 3a, the overall rate constants in different parts were calculated,  $K_{(\text{UV})} = \sim 0.27 \pm 0.02 \text{ s}^{-1}$  and  $K_{(\text{dark})} = \sim 0.15 \pm 0.02 \text{ s}^{-1}$ . Compared with those in pentacene OTFTs, PEDI OTFTs show a 2 orders of magnitude quicker detrapping process. This is because electrons expected to recombine trapped holes on the surface of  $\text{TiO}_2$  nanoparticles originate from the conductive channel of the n-type transistors that have the much higher electron density. The n-type OTFTs can endure the relatively long-term operation but gradually

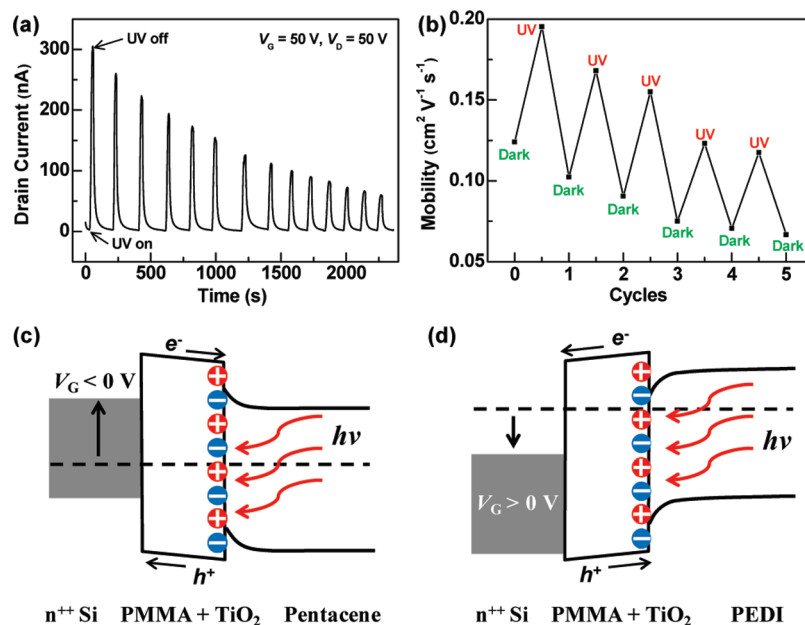


**Figure 3.** (a) Time trace of  $I_D$  for an n-type device used in Figure S10 (Supporting Information), showing the reversible charge trapping/detrapping processes under UV irradiation and in the dark.  $V_D = 50$  V, and  $V_G = 50$  V. (b) The corresponding representative five switching cycles of the mobility of the same device. (c, d) A possible model for the band diagrams and charge distribution in both p-type (c) and n-type (d) devices.

degrade after tens of cycles of UV irradiation, mainly due to the intrinsic instability of n-type semiconductors. Correspondingly, the device can nicely toggle its electron mobility back and forth between two distinct states many times. Figure 3b shows such a representative five cycles of the mobility transition. A series of control experiments similar to those used for pentacene transistors are presented in the Supporting Information (Figure S11–13). These control experiments consistently support that charge trapping/detrapping processes at the semiconductor/dielectric interface play the key role in device characteristics.

A possible model of the band bending situation and processes involved is presented in Figure 3c,d in order to clearly explain the phenomena in both p-type (Figure 3c) and n-type (Figure 3d) devices. At UV light turn-on, the light-sensitive  $\text{TiO}_2$  nanoparticles at the interface can generate the free electron–hole pairs when the photon energy is absorbed by them. The photogenerated holes and electrons behave differently. The holes are easily trapped inside of  $\text{TiO}_2$  nanoparticles, while the electrons can flow through the thin dielectric layer.<sup>33</sup> Under a negative gate bias, the electrons move toward the semiconductor/dielectric interface and behave like a Coulomb trap to lower the hole-carrier mobility in the p-type semiconductors. Conversely, under a positive gate bias, the electrons flow toward the gate electrode, and the trapped holes act as a local positive gate voltage, thus increasing the electron-carrier mobility in the n-type semiconductors. On the basis of this understanding, it would be very interesting to probe the charge trapping/detrapping process at the interface in a single ambipolar device, which shows both electron- and hole-transport properties.

A typical ambipolar device based on pentacene and PEDI semiconductors was fabricated through two sequential

thermal evaporations (Figure S14, Supporting Information). Figure S14 (Supporting Information) shows the output characteristics of a representative ambipolar device measured in air at room temperature. At high gate voltage ( $|V_G|$ ) and low source–drain voltage ( $|V_D|$ ), the device worked as a unipolar transistor in either the electron or hole accumulation mode. At low  $|V_G|$  and the relatively higher  $|V_D|$ , the electrons and holes were accumulated in their respective channels, resulting in the increase of the drain current with the increase of  $|V_D|$ , which confirmed the occurrence of its bipolar operation. Figure S14b (Supporting Information) shows the transfer characteristics of the same device at the different source–drain voltage biases. These curves show the V-shaped characteristics, which confirms the efficient bipolar behavior, with one arm for electron transport and the other for hole transport. According to the transfer curve of the device at  $V_D = 100$  V, the hole and electron mobilities were calculated,  $\mu_{(\text{hole})} = \sim 0.23 \text{ cm}^2 \text{ V}^{-1} \text{ s}^{-1}$  and  $\mu_{(\text{electron})} = \sim 0.11 \text{ cm}^2 \text{ V}^{-1} \text{ s}^{-1}$ . These values are comparable to those in separate p-type or n-type transistors that we used above and in the literature.<sup>2,3,35</sup>

Figure 4a–c shows the time traces of the charge trapping/detrapping process when the same ambipolar device was held at different gate biases and at a constant source–drain bias (40 V). At the negative gate voltages where the hole carriers dominate charge transport in devices, the photogenerated electrons can trap the hole carriers flowing through the conductive channel, thus leading to the significant conductance decrease (Figure 4a). The change in drain current ( $|\Delta I_D|$ ) at  $V_G = -100$  V is higher than that at  $V_G = -40$  V and increases with the increase of the gate bias ( $|V_G|$ ) due to the availability of more charge carriers. However, when the positive gate voltages were applied, we observed an opposite,

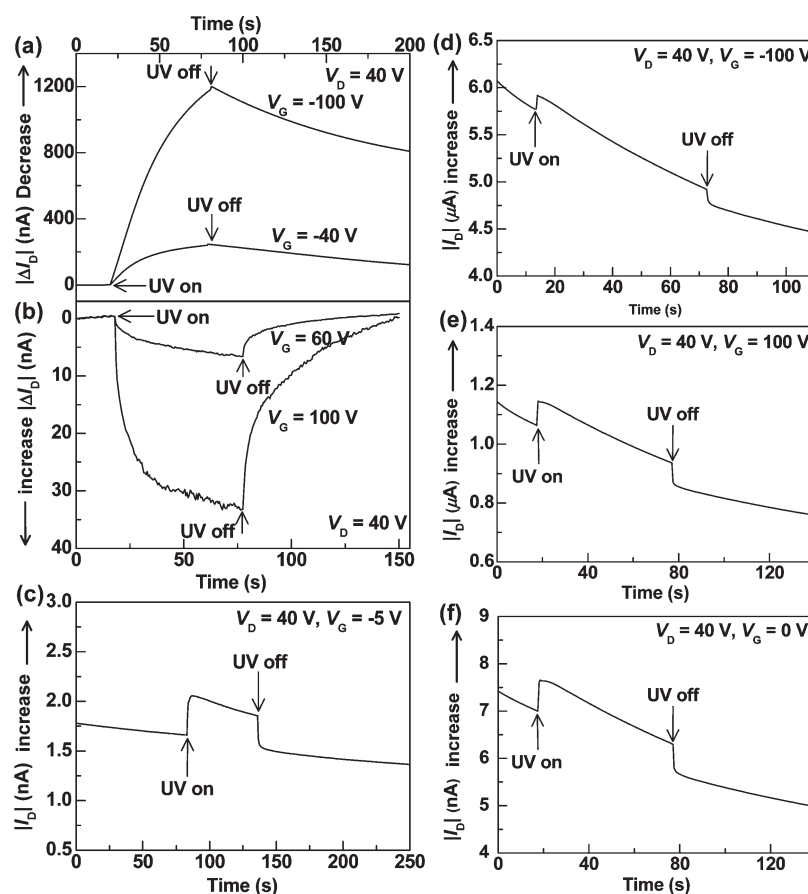


**Figure 4.** Time traces of  $I_D$  of an ambipolar device used in Figure S14 (Supporting Information) at negative (a) and positive (b) gate biases, showing symmetric, opposing photoswitching effects under UV illumination.  $V_D = 40$  V. (c) Time trace of  $I_D$  of the same device at  $V_G = -5$  V and  $V_D = 40$  V, only showing the sudden occurrence of the photocurrent at the moment of UV light turn-on. (d–f) The photoresponses of control experiments at the different gate voltage,  $V_G = -100$  V for (d), 100 V for (e), and 0 V for (f).  $V_D = 40$  V. More details of the control device can be found in the Supporting Information.

large current increase under UV irradiation (Figure 4b). As expected, this is because the photogenerated holes have an opposing function as a local gate voltage to increase the electron carriers in the n-type materials. Interestingly, at  $V_G = -5$  V, the transition point between electron and hole transport, we only observed the sudden occurrence of the photocurrent at the moment of UV light turn-on (Figure 4c) due to the photoexcitation of organic semiconductors. This is because the current decrease due to the trapping of hole carriers is offset by the current increase due to the enhancement of electron carriers in an ambipolar device at the transition state. These results are perfectly consistent with those described above. From the control experiment in Figure S15 (Supporting Information), we only found the simple, fast photocurrent jumps resulting from the photoexcitation of organic semiconductors at any gate voltage bias under UV irradiation (Figure 4d–f). These results strongly support that the photoexcitation and charge separation of  $\text{TiO}_2$  nanoparticles are responsible for the charge trapping/detrapping process at the interface in our devices. It is remarkable that tuning the photoactivity of  $\text{TiO}_2$  nanoparticles realizes symmetric, opposing photoswitching effects, which are effectively mirror images, in a single ambipolar OTFT.

This study provides a stark example of how interfacial engineering functions as an effective approach to improving device performance and/or installing new functionalities in organic optoelectronic devices. It highlights the vital importance of charge trapping/detrapping processes at the semiconductor/dielectric interface to the device performance of OTFTs. In great detail, we studied the optoelectronic properties of organic field-effect transistors using photoactive  $\text{TiO}_2$  nanoparticles combined with polymer PMMA as hybrid gate dielectrics. This approach allows us to perform the first dynamical investigation of charge trapping/detrapping processes at the photoactive polymer/semiconductor interface using OTFTs as local probes. By taking advantage of photoexcitation and charge separation of  $\text{TiO}_2$  nanoparticles, we found that the photogenerated electrons can serve as the trapping centers for quenching the hole carriers and thus lowering the mobility in a p-type semiconductor, and on the contrary, the photogenerated holes function as a local positive gate potential for improving the electron mobility in an n-type semiconductor. Importantly, when UV light was switched on/off, we were able to reversibly modulate charge trapping/detrapping processes at the interface and consequently fine-tune the device characteristics of both p-type and n-type OTFTs

in the opposite directions. Finally, it is remarkable to note that rational utilization of the charge dynamics at the interface afforded symmetric, opposite photoswitching effects in a single ambipolar OTFT. We believe that these results provide the deeper understanding of interfacial phenomena and offer new attractive insight for building the future practical/multifunctional molecular devices through better usage of the interfacial properties and rational development of novel interface modification approaches.

**SUPPORTING INFORMATION AVAILABLE** Data for AFM images, data for the TEM image of TiO<sub>2</sub> nanoparticles, data for X-ray diffraction experiments, and data for control experiments mentioned in the text. This material is available free of charge via the Internet at <http://pubs.acs.org>.

#### AUTHOR INFORMATION

##### Corresponding Author:

\*To whom correspondence should be addressed. E-mail: [guoxf@pku.edu.cn](mailto:guoxf@pku.edu.cn).

**ACKNOWLEDGMENT** We acknowledge primary financial support from FANEDD (No. 2007B21 and 2009A01), MOST (2009-CB623703 and 2008AA062503), and NSFC (Grant No. 50873004, 50821061, and 20833001).

#### REFERENCES

- Dimitrakopoulos, C. D.; Malenfant, P. R. L. Organic Thin Film Transistors for Large Area Electronics. *Adv. Mater.* **2002**, *14*, 99–117.
- Murphy, A. R.; Frechet, J. M. J. Organic Semiconducting Oligomers for Use in Thin Film Transistors. *Chem. Rev.* **2007**, *107*, 1066–1096.
- Zaumseil, J.; Sirringhaus, H. Electron and Ambipolar Transport in Organic Field-Effect Transistors. *Chem. Rev.* **2007**, *107*, 1296–1323.
- Kagan, C. R.; Andry, P. *Thin-Film Transistors*; Dekker: New York, 2003.
- Reese, C.; Bao, Z. Organic Single-Crystal Field-Effect Transistors. *Mater. Today* **2007**, *10*, 20–27.
- DiBenedetto, S. A.; Facchetti, A.; Ratner, M. A.; Marks, T. J. Molecular Self-Assembled Monolayers and Multilayers for Organic and Unconventional Inorganic Thin-Film Transistor Applications. *Adv. Mater.* **2009**, *21*, 1407–1433.
- Tang, Q.; Jiang, L.; Tong, Y.; Li, H.; Liu, Y.; Wang, Z.; Hu, W.; Liu, Y.; Zhu, D. Micrometer- and Nanometer-Sized Organic Single-Crystalline Transistors. *Adv. Mater.* **2008**, *20*, 2947–2951.
- Cao, Y.; Steigerwald, M. L.; Nuckolls, C.; Guo, X. Current Trends in Shrinking the Channel Length of Organic Transistors Down to the Nanoscale. *Adv. Mater.* **2010**, *22*, 20–32.
- Sirringhaus, H. Device Physics of Solution-Processed Organic Field-Effect Transistors. *Adv. Mater.* **2005**, *17*, 2411–2425.
- Di, C.-A.; Liu, Y.; Yu, G.; Zhu, D. Interface Engineering: An Effective Approach toward High-Performance Organic Field-Effect Transistors. *Acc. Chem. Res.* **2009**, *42*, 1573–1583.
- Jurchescu, O. D.; Popinciuc, M.; van Wees, B. J.; Palstra, T. T. M. Interface-Controlled, High-Mobility Organic Transistors. *Adv. Mater.* **2007**, *19*, 688–692.
- Chua, L.-L.; Zaumseil, J.; Chang, J.-F.; Ou, E. C. W.; Ho, P. K. H.; Sirringhaus, H.; Friend, R. H. General Observation of N-Type Field-Effect Behaviour in Organic Semiconductors. *Nature* **2005**, *434*, 194–199.
- Tseng, C.-W.; Tao, Y.-T. Electric Bistability in Pentacene Film-Based Transistor Embedding Gold Nanoparticles. *J. Am. Chem. Soc.* **2009**, *131*, 12441–12450.
- Bredas, J. L.; Calbert, J. P.; Da Silva Filho, D. A.; Cornil, J. Organic Semiconductors: A Theoretical Characterization of the Basic Parameters Governing Charge Transport. *Proc. Natl. Acad. Sci. U.S.A.* **2002**, *99*, 5804–5809.
- Yan, H.; Chen, Z.; Zheng, Y.; Newman, C. E.; Quin, J.; Dolz, F.; Kastler, M.; Facchetti, A. A High-Mobility Electron-Transporting Polymer for Printed Transistors. *Nature* **2009**, *457*, 679–686.
- Guo, X.; Xiao, S.; Myers, M.; Miao, Q.; Steigerwald, M. L.; Nuckolls, C. Photoresponsive Nanoscale Columnar Transistors. *Proc. Natl. Acad. Sci. U.S.A.* **2009**, *106*, 691–696.
- Salleo, A.; Street, R. A. Light-Induced Bias Stress Reversal in Polyfluorene Thin-Film Transistors. *J. Appl. Phys.* **2003**, *94*, 471–479.
- Miyadera, T.; Wang, S. D.; Minari, T.; Tsukagoshi, K.; Aoyagi, Y. Charge Trapping Induced Current Instability in Pentacene Thin Film Transistors: Trapping Barrier and Effect of Surface Treatment. *Appl. Phys. Lett.* **2008**, *93*, 033304/1–033304/3.
- Wang, S. D.; Minari, T.; Miyadera, T.; Aoyagi, Y.; Tsukagoshi, K. Bias Stress Instability in Pentacene Thin Film Transistors: Contact Resistance Change and Channel Threshold Voltage Shift. *Appl. Phys. Lett.* **2008**, *92*, 063305/1–063305/3.
- Richards, T.; Sirringhaus, H. Bias-Stress Induced Contact and Channel Degradation in Staggered and Coplanar Organic Field-Effect Transistors. *Appl. Phys. Lett.* **2008**, *92*, 023512/1–023512/3.
- Miyadera, T.; Minari, T.; Wang, S. D.; Tsukagoshi, K. Dynamic Bias Stress Current Instability Caused by Charge Trapping and Detrapping in Pentacene Thin Film Transistors. *Appl. Phys. Lett.* **2008**, *93*, 213302/1–213302/3.
- Qiu, Y.; Hu, Y.; Dong, G.; Wang, L.; Xie, J.; Ma, Y. H<sub>2</sub>O Effect on the Stability of Organic Thin-Film Field-Effect Transistors. *Appl. Phys. Lett.* **2003**, *83*, 1644–1646.
- Zhu, Z.-T.; Mason, J. T.; Dieckmann, R.; Malliaras, G. G. Humidity Sensors Based on Pentacene Thin-Film Transistors. *Appl. Phys. Lett.* **2002**, *81*, 4643–4645.
- Zilker, S. J.; Detcheverry, C.; Cantatore, E.; de Leeuw, D. M. Bias Stress in Organic Thin-Film Transistors and Logic Gates. *Appl. Phys. Lett.* **2001**, *79*, 1124–1126.
- Salleo, A.; Endicott, F.; Street, R. A. Reversible and Irreversible Trapping at Room Temperature in Poly(thiophene) Thin-Film Transistors. *Appl. Phys. Lett.* **2005**, *86*, 263505/1–263505/3.
- Kagan, C. R.; Afzali, A.; Martel, R.; Gignac, L. M.; Solomon, P. M.; Schrott, A. G.; Ek, B. Evaluations and Considerations for Self-Assembled Monolayer Field-Effect Transistors. *Nano Lett.* **2003**, *3*, 119–124.
- Klauk, H.; Zschieschang, U.; Pflaum, J.; Halik, M. Ultralow-Power Organic Complementary Circuits. *Nature* **2007**, *445*, 745–748.
- Ohko, Y.; Tatsuma, T.; Fujii, T.; Naoi, K.; Niwa, C.; Kubota, Y.; Fujishima, A. Multicolour Photochromism of TiO<sub>2</sub> Films Loaded with Silver Nanoparticles. *Nat. Mater.* **2003**, *2*, 29–31.
- Hoffmann, M. R.; Martin, S. T.; Choi, W.; Bahnemann, D. W. Environmental Applications of Semiconductor Photocatalysis. *Chem. Rev.* **1995**, *95*, 69–96.

- (30) Lee, W.-H.; Wang, C. C.; Ho, J. C. Influence of Nano-composite Gate Dielectrics on OTFT Characteristics. *Thin Solid Films* **2009**, *517*, 5305–5310.
- (31) Yan, F.; Li, J.; Mok, S. M. *J. Appl. Phys.* **2009**, *106*, 074501/1–074501/7.
- (32) Cho, S.; Seo, J. H.; Lee, K.; Heeger, A. J. Enhanced Performance of Fullerene n-Channel Field-Effect Transistors with Titanium Sub-Oxide Injection Layer. *Adv. Funct. Mater.* **2009**, *19*, 1459–1464.
- (33) Dittrich, T.; Duzhko, V.; Koch, F.; Kytin, V.; Rappich, J. Trap-Limited Photovoltage in Ultrathin Metal Oxide Layers. *Phys. Rev. B* **2002**, *65*, 155319/1–155319/5.
- (34) Calhoun, M. F.; Hsieh, C.; Podzorov, V. Effect of Interfacial Shallow Traps on Polaron Transport at the Surface of Organic Semiconductors. *Phys. Rev. Lett.* **2007**, *98*, 096402/1–096402/4.
- (35) Chesterfield, R. J.; McKeen, J. C.; Newman, C. R.; Ewbank, P. C.; da Silva, D. A.; Bredas, J. L.; Miller, L. L.; Mann, K. R.; Frisbie, C. D. Organic Thin Film Transistors Based on *N*-Alkyl Perylene Diimides: Charge Transport Kinetics as a Function of Gate Voltage and Temperature. *J. Phys. Chem. B* **2004**, *108*, 19281–19292.